paper reference: 10.12

MODELING OF DUCTILE TEARING OF PIPELINE–STEEL WIDE PLATES

J. Besson[1], F. Rivalin[1], M. Di Fant[2], A. Pineau'

[1] Ecole des Mines de Paris, Centre des Matériaux, UMR CNRS 7633
BP 87, 91003 Evry Cedex, France
[2] Irsid Maizières les Metz, Cedex, France

ABSTRACT

The fracture resistance of steel plates used to build pipelines is commonly characterized by measuring macroscopic rupture parameters such as the energy dissipation rate, the thickness reduction or the crack opening angle. In this study, the local approach to fracture is used to modcl tests carried out on wide plates and to predict global parameters.

The proposed model is based on an extension of the Gurson model including plastic anisotropy and viscosity. The mechanical behavior of the material is characterized using tensile bars tested along different directions. Rupture is characterized using notched bars. The inclusion content is measured using metallography.

The model is used to numerically investigate the effect of plate thickness, through thickness hardness gradients and plastic anisotropy on the fracture resistance.

INTRODUCTION

In order to maintain structural integrity of components such as large–diameter pipelines and to prevent fracture by unstable longitudinal dynamic propagation of cracks, a minimum toughness lcvcl is rcquired for pipeline steels. It is usually assessed from the Charpy–V fracture toughness tests, Drop Weight Tear Tests or full–scale burst tests [1]. On the other hand, attempts have been made to calculate crack propagation and crack arrest in pipeline by the numerical computation of pipeline burst and decompression [2].

In these numerical studies, the problem of the material fracture criteria remains a key issue. Global parameters such as a critical Crack Tip Opening Angle (CTOA), or a critical dissipated energy proved to be dependent, of the specimen and loading configuration. Similar difficulties are encountered in the more general framework of the so–called "global approach to fracture". Global parameters such as the J-integral or the more recently introduced constraint factor Q [3]are unable to capture experimentally observed geometry effects. On the other hand, the "local approach to fracture" is thought to be able to deal with those problems as it is based on a micromechanical description of the mechanisms involved in the fracture process [4].

The aim of this paper is to demonstrate the ability of fully–coupled local approach of ductile fracture to simulate crack propagation over long distances. For this purpose, a rolled ferrito–pearlitic steel was investigated using static and dynamic ductile tearing experiments. Tests were carried out on wide plates allowing for crack advances over 200 mm. The mechanical and damage behavior of the rnaterial was characterized using tensile specimens and notched bars.

The constitutive equations describing the material are based on the Gurson model [5] which has been extended to account for plastic anisotropy and viscous effects. Finite Element simulations are used to simulate ductile tearing tests. Simulations are restricted to static in plane propagation. Shear bands arc observed during dynamic tests. The influence of computational parameters such as mesh size, element shape are also studied in order to check the validity of the simulations. The model is applied to simulate crack propagation over long distances (i.e. > 100 mm). The model is used to predict fracture global parameters such as the energy dissipation rate, R, proposed by Klemm [6] and Turner [7], the thickness reduction ratio at fracture, Z and the CTOA. In particular, the cffcct of the sheet thickness on R and Z is investigated.

CONSTITUTIVE EQUATIONS — ANISOTROPIC GURSON MODEL

In order to represent the plastic and damage behavior of the investigated steel, an extension of the Gurson-Tvcrgaard-Needleman (GTN) model including plastic anisotropy and visco–plastic effects is proposed. An effective scalar stress $\sigma_\star$ is implicitly defined by the following equation:

$$\left(\frac{\sigma_H}{\sigma_\star}\right)^2 + 2q_1 f_\star \cosh\left(\frac{3}{2}q_2\frac{\sigma_m}{\sigma_\star}\right) - 1 - q_1^2 f_\star^2 = 0 \tag{1}$$

σ_H is the Hill equivalent stress and σ_m the mean stress. q_1 and q_2 are constant parameters introduced on a phenomenological basis so that the model closely corresponds to unit cell calculations. $f_\star$ is an effective porosity. It is a function of the actual porosity f which has been introduced by Tvergaard and Needleman (GTN modcl) to represent void coalescence leading to final fracture. It is assumed that coalescence starts at a critical porosity f_c. For actual porosities f larger than f_c, the mechanical softening due to void growth is larger than what is predicted by the original Gurson model. Based on these assumptions, the simplest phenomenological form for $f_\star$ is expressed as :

$$f_\star = \begin{cases} f & \text{if } f < f_c \\ f_c + \delta\,(f - f_c) & \text{if } f > f_c \end{cases} \tag{2}$$

where S > 1 is a coefficient representing the increased damaging effect of porosity. Both f_c and 6 have to be adjusted. Failure occurs when $f_\star = 1/q_1$. The flow potential Φ is then defined as:

$$\Phi = \sigma_\star - R \tag{3}$$

where R is the yield stress of the undamaged material depending on the matrix cumulated plastic strain p. In the case of plastic flow, the yield condition is expressed as $\Phi = 0$. The present formulation is then equivalent to the standard formulation of the Gurson model in which equation 1 is considered as the yield condition. In the case of viscoplasticity, flow occurs for $\Phi \geq 0$. The difference $\sigma_\star$ – R is then considered as an effective creep stress.

In order to account for the plastic anisotropy of the material, the von Mises equivalent stress σ_e (used in the standard GTN model) has been replaced by the Hill equivalent stress σ_H in equation 1 : σ_H is defined as:

$$\sigma_H = \sqrt{\frac{3}{2}\,\underset{\sim}{\mathbf{s}} : \underset{\approx}{\mathbf{H}} : \underset{\sim}{\mathbf{s}}} \tag{4}$$

where $\underset{\sim}{\mathbf{s}}$ is the stress deviator and $\underset{\approx}{\mathbf{H}}$ the Hill anisotropy fourth order tensor. When writing σ_H in the anisotropy principal axes, which, in the case of the study, correspond to S = Short Transverse

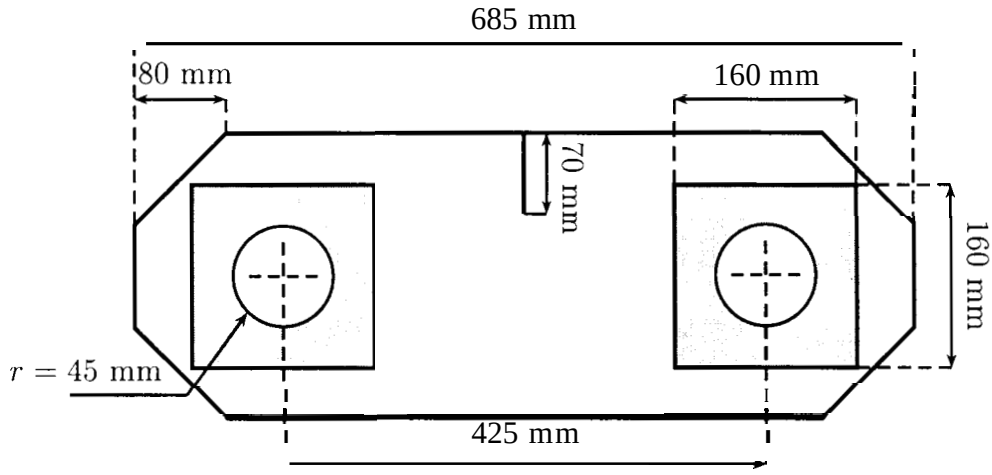

Figure 1: Wide plate specimen. Shaded areas represent welded reinforcements used to prevent plastic collapse in the loading region

(thickness), T = Transverse (perpendicular to rolling direction) and L = Long (parallel to rolling direction) directions, σ_H has the following expression:

$$\sigma_H^2 = \frac{3}{2}\left(h_{\mathrm{SS}} s_{\mathrm{SS}}^2 + h_{\mathrm{TT}} s_{\mathrm{TT}}^2 + h_{\mathrm{LL}} s_{\mathrm{LL}}^2 + 2h_{\mathrm{ST}} s_{\mathrm{ST}}^2 + 2h_{\mathrm{TL}} s_{\mathrm{TL}}^2 + 2h_{\mathrm{SL}} s_{\mathrm{SL}}^2\right) \tag{5}$$

This modification of the Gurson model is purely phenomenological. It only affects the contribution of deviatoric stresses on the potential definition. The role of pressure *(a,)* in the modified potential remains the same as in the original Gurson model. Damage is still assumed to be isotropic.

MATERIAL TESTING — MATERIAL PARAMETERS

The material of this study is a X70 ferritic pearlitic steel. It belongs to the HSLA (High Strain Low Alloyed) steel family, micro–alloyed with niobium and vanadium. Investigation of the inclusions by image analysis of polished surfaces as well as X–ray analysis revealed a very low inclusion volume fraction (about $1.5 \,.\, 10^{-4}$) which is related to the very low sulphur and phosphorus content. The inclusion population is characterized by small, globular particles of low mean diameter (about 1pm), composed of two phases combining calcium sulfide CaS and aluminum or magnesium oxides [8].

The mechanical behavior was investigated using standard test samples including smooth and notched round tensile bars. Crack propagation over long distances was studied using wide plates (685mm×250mm) with a lateral saw–machined notch. These plates were tested using a 2500 kN tensile machine under quasi–static conditions (ram speed $0.1\,\mathrm{mm.s^{-1}}$). Under these conditions, fracture surfaces are flat and perpendicular to the loading direction. Note that under dynamic conditions, shear fracture is observed. **A** schematic drawing of the specimen is shown on figure 1.

Materials parameters (gathered in table 1) can be divided in two different sets: (i) parameters relative to the (visco)–plastic behavior, (ii) parameters relative to damage and rupture behavior. Due to the very low inclusion volume fraction, damage has very little effect on the overall plastic behavior until the plastic strain reaches $\approx$ 20%. It was therefore possible to independently determine the first set of parameters using tensile specimens along 6 directions of the plate including three out–of–plane directions (L, T, S, LT, TS, SL). The hardening behavior is described using a simple power law relationship:

$$R(p) = K\,(p + \varepsilon_0)^n \tag{6}$$

TABLE 1
MODEL PARAMETERS

Elasticity	Young's modulus: 210 GPa, Poisson's ratio: 0.3
Plastic hardening	$K = 795$ MPa, $n = 0.13$, $\varepsilon_0 = 0.002$
Viscoplasticity	$IS = 55$ MPa.s$^{1/n'}$, $n' = 5$
Hill criterion	$h_{\mathrm{LL}} = 1.185, h_{\mathrm{TT}} = 0.823$, $h_{\mathrm{SS}} = 1.552$,
	$h_{\mathrm{LT}} = 1.586, h_{\mathrm{TS}} = 1.896, h_{\mathrm{SL}} = 0.801$
GTN	$f_0 = 1.5\,10^{-4}$, $f_c = 7.4\,10^{-4}$, $\delta = 3.8$
Element, thickness	$h_T = 1\,\mathrm{mm}$

The viscoplastic behavior was characterized using a Norton law:

$$\dot{p} = \left\langle \frac{\sigma_H - R(p)}{K'} \right\rangle^{n'} \tag{7}$$

In particular, it can be noted that $h_{,,}$ is much larger than $h_{,,}$ and h_{TT}. This indicates that, in a tensile test along the L (resp. T) direction, the investigated material deforms more along the S direction than along the T (resp. L) direction, as observed experimentally.

The initial void volume fraction f_0 was taken as being the inclusion (CaS+oxides) volume fraction [8]. It was thus assumed that immediate debonding between the matrix and the inclusions takes place. Damage parameters of the Gurson–type model (f_c and 6) have to be determined by comparing experiments with FE simulations. For this purpose, axisymmetric notched bars were used. The minimum diarneter, ϕ_0, and the outer diameter, $,were equal to 10 mm and 18 mm, respectively, while the notch radius was taken equal to **4** and 2 mm Reducing the notch radius increases the stress triaxiality ratio in the minimum section and leads to lower strains to failure. To perform the identification of f_c and 6, experimental normalized forces F/S_0 (F: force, S_0: initial minimum cross section) and radial displacement along the L direction $\Delta\phi_{\mathrm{L}}$ were compared with Finite Element (FE) simulations. Note that due to strong anisotropic behavior of the material, three–dimensional calculations are rcquired. f_c and S were adjusted to reproduce the sharp drop of the load which corresponds to the initiation of a central crack in the specimens.

In order to model crack propagation, it is necessary to adjust a characteristic length. In practice, this length is defined by selecting a proper mesh size [9]. Test calculations have shown that the element size in the direction perpendicular to the crack plane, has the greatest influence. In the present case, cracks propagate along the L–direction in the L–S plane. The corresponding length is the clement size along the transverse direction $h_{,}$. It was adjusted in order to represent the experimental energy dissipation rate R.

NUMERICAL PROCEDURES

The modified GTN model was implemented in the FE software Zébulon, developed at Ecole des Mines de Paris [10]. An implicit scheme is used to integrate the constitutive equations. The consistent tangent matrix is computed using the method proposed in [11]. As the material is anisotropic, the simplified method proposed by Aravas [12] cannot be used. The material is considered as broken when $f_\star$ reaches $1/q_1 - \varepsilon$ with $\varepsilon = 10^{-3}$. In that case, the behavior is replaced by an elastic behavior with a very low stiffness (Young's modulus: $E_b = 1\,\mathrm{MPa}$). Calculations were done using quadratic elements with reduced integration. Plane stress (PS), plane strain (PE) and 3D elements were used. In regions where the crack propagates, 8 nodes (PS and PE) and 20 nodes (3D) elements were used. An updated Lagrangian formulation was used in which Jauman stress rates are used.

An example of the FE meshes used to simulate ductile tearing of wide plates is shown on figure 2. The initial thickness of the plate is referred to as B_0. Due to the symrnetries of the problem, one fourth of the specimen is meshed. In some cases, combined 2D/3D meshes were used. This technique

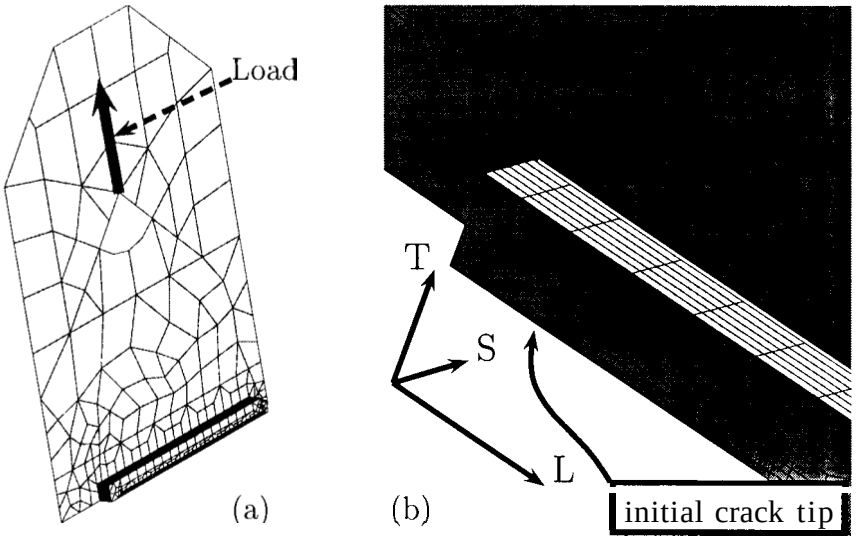

Figure 2: Meshes used for the FE simulations

reduces the number of degrees of freedom. The 2D part (plane stress) is used to load the specimen while the crack propagates in the 3D part. The number of elements used to mesh the thickness was varied between 1 and 6 in order to study the role of mesh refinement on the results.

RESULTS

Tests conducted on wide plate specimens were used to determine two macroscopic fracture parameters: (1) the energy dissipation rate R, (2) the thickness reduction ratio Z. They are defined as:

$$R = \frac{1}{B_0}\frac{dU}{da} \qquad Z = \frac{B_0 - B_R}{B_0} \tag{8}$$

where B_0 (resp. B_R) is the initial plate thickness (the plate thickness at rupture), a the crack length and U the dissipated energy. Tests have shown that both R and Z have almost constant values for crack advances between 50 and 140 mm.

Numerical simulation was used compute both R and Z. Three effects have been studied: (i) effect of the plate thickness, (ii) effect of a hardness gradient, (iii) effect of plastic anisotropy.

Mesh size sensitivity

The element thickness in the loading direction (T) was fixed to represent the experimental values of R. However element sizes in both other directions can also influence the numerical results. The maximum number of elements used to mesh the thickness is 6. The problem has then about 30000 degrees of freedom. The following conclusion can be drawn from the numerical investigations:

- Z: 6 elements in the thickness are required to obtained a good description of necking for a thickness equal to 20 mm. For $B_0 < 10$ mm results tend to be less sensitive as plane stress conditions prevail (e.g. for $B_0 = 10$ mm the same results are obtained for 2 and 3 elements). For large values of B_0, plane strain conditions dominate so that the results also become independent on the thickness discretization.
- R: Calculated values of R are much less sensitive to the thickness discretization. Large scale yielding is always observed so that the energy dissipated in the elements undergoing rupture (and consequently the highest thickness reduction) remains small compared to the total energy.
- h, Values of 2.5 and 5.0 mm were used for the element size in the propagation direction (h_L). No significant differences were found.

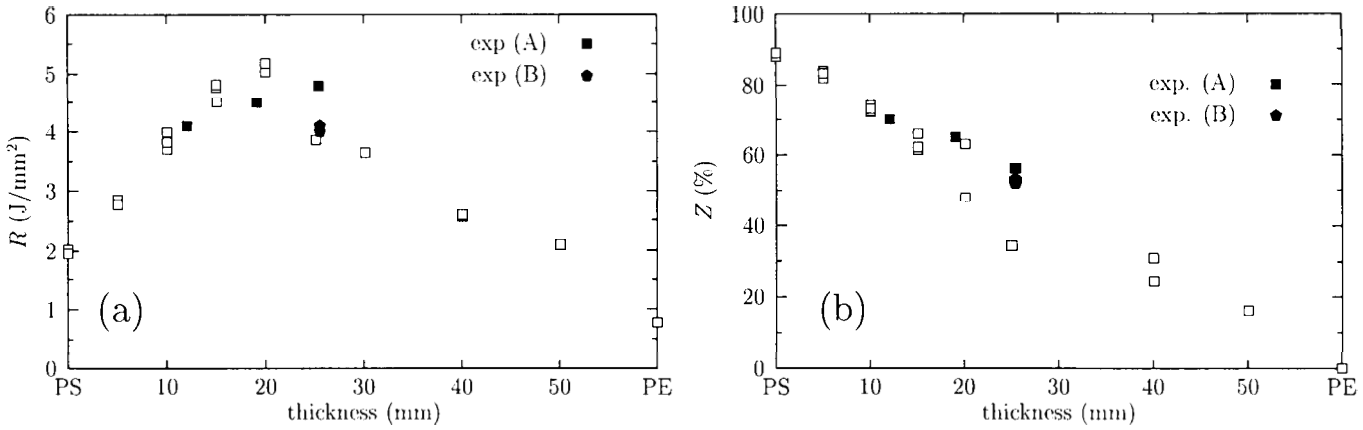

Figure **3:** Effect of the initial plate thickness B_0 on the energy dissipation rate (a) and the thickness reduction Z (b). Open symbols: simulations, closed symbols: experiments for two steels (A) and (B).

The elements used in this work remain however large in comparison with other studies [13, 14]. However considering the total simulated crack advance, the same number of elements/degrees of freedom are used to describe propagation. Based on the previous remarks, it appears that the present FE discretization is suitable to model the main experimental features and trends observed during propagation. It is clearly not fine enough to closely represent initiation.

Thickness effect

Figure **3** shows the variations of R and Z as a function of the initial thickness. For some thicknesses, several simulations were performed using different element size. FE simulations correctly represent the fact that R reaches a maximum (for B_0 **м** 20 mm) and are in reasonable agreement with the experiments. The evolution of R as a function of B_0 can be explained as follows. As thickness increases, the deformation condition along the thickness direction progressively changes from plane stress to plane strain. This results in an increase of the stress triaxiality ratio which has two antagonist effects: (i) higher stresses are generated in the loading direction leading to a higher dissipated energy : (ii) the void growth rate $\dot{f}$ is increased so that the critical porosity f_c is reached sooner. This results first in an increasing value of R (due to higher stresses) followed by a decrease (due to the accelerated void growth). On the other hand, Z is a continuously decreasing function of the thickness.

Through–thickness hardness gradient

Rolled plates can have a softer or harder outer surface [8]. In order to numerically investigate the effect of such a hardness gradient, calculations were performed under the following assumptions. The plate (thickness: 10 and 20 mm) is divided in bulk and a skin regions having the same volume. Bulk and skin are assumed to be either softer or harder ($\pm 30\%$) so that the average stress—strain curve (given by the law of mixture) in the loading direction remains constant. Three situations are therefore envisaged: (i) soft skin, hard bulk, (ii) hard skin, soft bulk, (iii) homogeneous material. All other properties are supposed to remain constant. It is shown on figure 4 that the higher R is obtained in the case where the plate has a hard skin ; the lowest value is obtained in the case of the soft skin. The opposite trend is observed for the thickness reduction Z. FE analysis shows that a hard skin prornotes a more homogeneous stress state along the thickness direction together with a lower stress triaxiality in the middle of the plate. In this case, the crack front tends to be flatter as shown on figure 5.

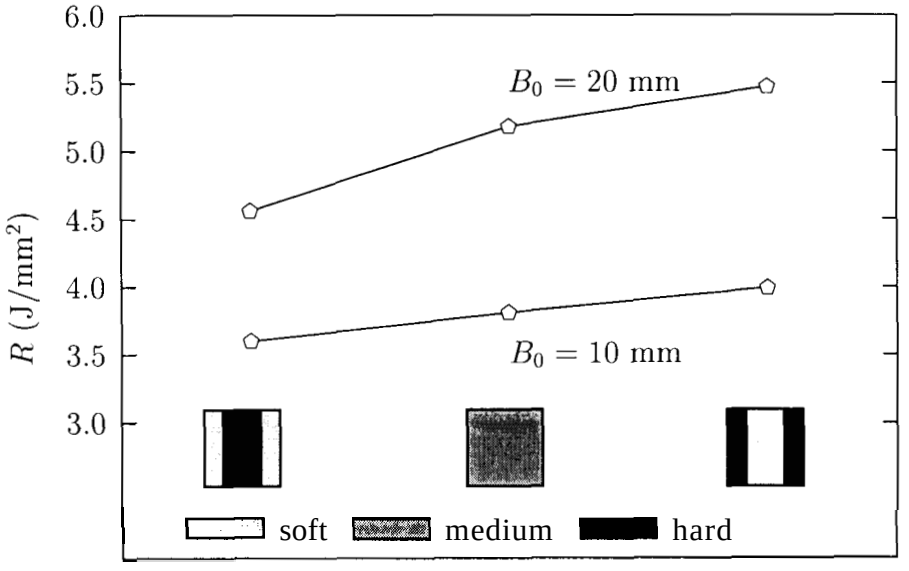

Figure 4: Effect of through–thickness hardness gradients on the energy dissipation rate (R).

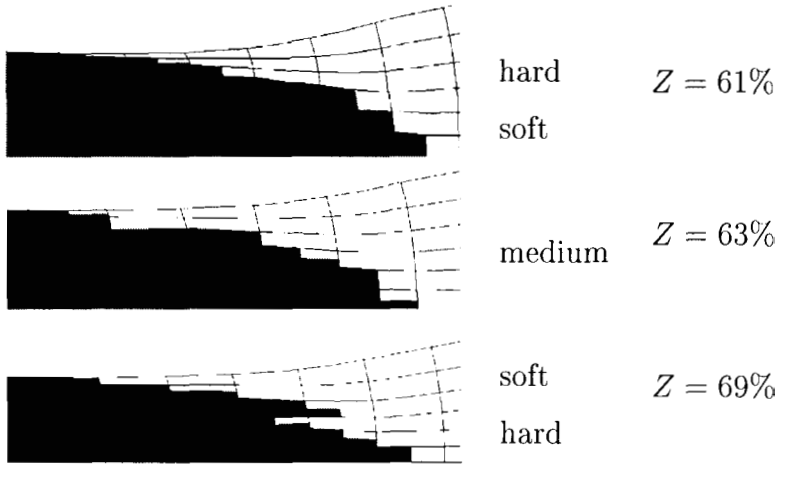

Figure 5: Crack front (gray) for different hardness profiles.

Plastic **anisotropy**

Experiments carried out on plates (thickness: 25.4 mm) under quasi–static conditions have shown that the crack growth resistance depends on the loading direction [8]. Tests in the T—L orientation (i.e. T: loading direction, L: crack growth direction) give an average value of R equal to 4.05 J/mm^2 and an average value of Z equal to 52%. Tests in the L—T orientation (i.e. L: loading direction, T: crack growth direction) give the following values: R = 4.45 J/mm^2, Z = 64%. This indicates that the T—L orientation is less resistant than the L—T orientation. In order to interpret these results, FE simulations were carried out in the T—L and L—T orientations. A fictitious isotropic material was also adopted. In these additional 3D calculations, it was assumed that the values of f_0, f_c and δ were the same as those used previously. The plate thickness is equal to 25.4 mm using 2 elements along the thickness. Results are the following:

	T—L	L—T	Isotropic
Z (%)	34	44	21
R (J/mm^2)	3.9	5.1	2.2

As for the experiments, the plate is tougher when tested in the L–T orientation than in the T–L orientation: both R and Z are increasing. The isotropic material exhibits a strongly reduction of resistance. This is correlated with a sharper neck (although Z is smaller) which increases the stress triaxiality ratio in the center of the plate. Similar geometrical effects are observed when comparing L–T and T—L orientations. Ductile tearing anisotropy may indeed be caused by purely metallurgical parameters such as inclusion anisotropic shape, or anisotropic inclusion distribution. However, the present results show that plastic anisotropy alone can play an important role on the ductile tearing of plates.

CONCLUSIONS

In this work the local approach to fracture has been used to model the crack propagation over long distances in wide plates. The rnodel is based on an extended Gurson type model including the description of plastic anisotropy and viscosity. The model can be used to represent the observed effect of plate thickness on macroscopic fracture parameters (R and Z). The model can also be used to numerically investigate the effect of hardness gradients or plastic anisotropy and to propose solutions to optimize the processing of sheet materials.

References

1. Wiedenhoff, W.W., Vogt, G.H., Peters P.A. (1984) In *International Seminar on Fracture in Gas Pipelines,* pages 95–117, Moscou.
2. O'Donoghue, P.E., Green, S.T., Kanninen, M.F., Bowles, P.K. (1991) *Computers and Structures,* **38,** 501.
3. O'Dowd, N.P., Shih, C.F. (1992) *J. Mech. Phys. Solids,* **40,** 939.
4. Pineau, A. (1992) In A.S. Argon, editor, *Topics in Fracture and Fatigue,* pp. 197–234. Springer Verlag Inc., NY.
5. Tvergaard, V. (1990) *Advances in Applied Mechanics,* **27,** 83.
6. Klernm, W. (1989) In H. Homma, D.A. Shockey, and G. Yagawa, editors, *Dynamic fracture mechanics for the 1990s,* pp 99–104.
7. Turner., C.E. (1992) In *Fracture behavior and design* of *materials and structures/ECF 8,* pp. 933–968.
8. Rivalin, F. (1998) PhD thesis, Ecole des Mines de Paris, France.
9. Xia., L., Shih, C.F., Hutchinson, J.W. (1995) *J. Mech. Phys. Solids,* **43,** 389.
10. Besson, J., Le Riche, R., Foerch, R., Cailletaud, G. (1998) *Revue européenne des éléments finis,* **7,** 567.
11. Simo, J.C., Taylor, R.L. (1985) *Computer Methods in Applied Mechanics and Engineering,* **48,** 101.
12. Aravas, N. (1987) *Int. J. Num. Math. Engng,* **24,** 1395.
13. Yan, W.-Y., Kolednik, O., Fisher, F.D. (1998) pp. 1041–1046. In *ECF 12, Fracture from defect*
14. Skallerud, D. and Zhang, Z.L. (1999) pp 201–214. In *Fatigue and fracture mechanics,* ASTM STP 1332.